Acta Cryst. (1999). B**55**, 192–202

Charge and momentum densities of cubic tetracyanoethylene and its insertion compounds

Dominique Bélemlilga, Jean-Michel Gillet* and Pierre J. Becker

Laboratoire des Structures Electroniques et Modélisations, Ecole Centrale des Arts et Manufactures de Paris, Grande Voie des Vignes, 92295 Chatenay Malabry CEDEX, France. E-mail: gillet@sem.ecp.fr

(*Received 13 January 1998; accepted 23 September 1998*)

Abstract

Charge and momentum electron densities provide complementary views of cohesive forces in solids. This is particularly true for molecular crystals. The examples of cubic tetracyanoethylene (1,1,2,2-ethenetetracarbonitrile) and its alkali-metal insertion compounds are analyzed from a theoretical point of view. Besides the usual deformation density maps and anisotropy of Compton profiles, it is shown that interaction charge density and interaction Compton profiles can be defined and reveal the subtleties of the intermolecular interactions. It is shown that owing to the large cavities in the crystal, alkali-metal atoms can be inserted, leading to a strong charge transfer to the molecules and to a metallic character; the mechanism of insertion is revealed well by the combination of charge and momentum density studies. The combination of the two techniques of X-ray diffraction and Compton scattering should be of great help in the study of rather weak interactions present in molecular solids.

1. Introduction

Tetracyanoethylene (TCNE) is a highly symmetric organic molecule with three types of bonds (point group D_{2h}). It is also an electron acceptor and forms charge transfer complexes with a large variety of organic molecules (benzene, indene, cyclophanes *etc.*) (Looney & Downing, 1958; Webster *et al.*, 1962; Dhar, 1967; Matthews *et al.*, 1971; Czuchajowski *et al.*, 1974; Regnault, 1986; Edwards *et al.*, 1990; Cioslowski *et al.*, 1991; Emery *et al.*, 1992; Cioslowski, 1994). The high electron affinity of TCNE comes from the electronegativity of the four cyanide groups.

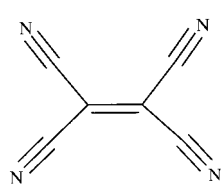

TCNE

Two crystallographic phases, cubic and monoclinic, were discovered by Bekoe & Trueblood (1960) and Little *et al.* (1971), respectively. The phase transition has been extensively studied using many experimental techniques (nuclear quadrupolar resonance, Raman and neutron scattering, dielectric measurements *etc.*) (Onda *et al.*, 1969; Murgich & Pissanetzky, 1975; Mierzejewski & Chaplot, 1980; Mukhopadhyay *et al.*, 1985). The transition from the monoclinic to the cubic phase occurs on heating to 318 K at atmospheric pressure. Phonon spectra for the cubic and monoclinic phases have been theoretically and experimentally analyzed by Chaplot and others (Chaplot *et al.*, 1983, 1985; van der Berg & van der Avoird, 1989) allowing the test of a semi-empirical atom–atom potential for molecular crystals. The valence electron distribution of cubic TCNE has been studied by combined X-ray and neutron scattering (Becker *et al.*, 1973).

In the cubic form of TCNE (Fig. 1) there is a cavity of diameter 7 Å in which atoms or molecules can be included, which allows the existence of a large number of organic complexes with various physical properties. Other organic solids also possess unoccupied sites in the crystalline state, leading to insertion compounds with interesting electronic properties. A recent example is provided by C_{60}; when combined with potassium, it leads to either a superconductor (K_3C_{60}) or an insulator (K_6C_{60}) (Erwin & Pederson, 1991; Erwin & Pickett, 1991; Hebard, 1991; Moscovici, 1994). Graphite and its

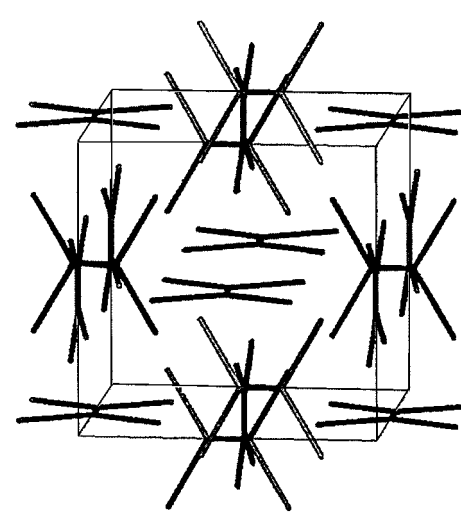

Fig. 1. Cubic TCNE.

ISSN 0108-7681

Table 1. *Molecular geometry of TCNE in the crystal and gas phases*

	Solid phase	Gas phase	
	Neutron diffraction	Electron diffraction	Hartree–Fock optimized geometry
Point group	D_{2h}	D_{2h}	D_{2h}
C—C (Å)	1.433 (2)	1.435 (10)	1.439
C═C (Å)	1.357 (3)	1.357 (10)	1.336
C≡N (Å)	1.166 (2)	1.162 (2)	1.131
C—C—C (°)	116.2 (2) (in plane)	117.8	116.32
C—C≡N (°)	178.1 (2) (in plane)		179.11

insertion compounds with alkali metals (Levi, 1977; Ohno *et al.*, 1979; Vincenzo & Rabii, 1982; Tatar, 1985; Moscovici, 1994) are other popular examples.

Although the idea of inserting atoms or small ions in the cavity of cubic TCNE was suggested by Little *et al.* (1971), no systematic study of the stability and electronic properties of such complexes has yet been performed. However, in the 1960s, Webster *et al.* (1962) established the existence of metal salts formed by TCNE with alkali-metal atoms and obtained crystals; unfortunately, the crystal structure was not solved.

This paper is devoted to the study of the electronic structure of cubic TCNE and its inclusion complexes with alkali-metal atoms (K or Na) from a band structure and electron density (in real and momentum spaces) point of view. It is organized as follows:

In §2, we discuss the geometry, stability and electronic behavior of cubic TCNE and its inclusion compounds in the Hartree–Fock approximation.

In §3, an analysis of band structures and density of states with the help of a Mulliken partitioning scheme is carried out; charge transfer properties and conduction mechanisms are clarified.

§4 is devoted to the charge and momentum densities of cubic TCNE and its inclusion compounds. We will define some simple functions and models that enable charge transfer mechanisms to be studied for insertion compounds.

To conclude, C_{60} and TCNE insertion compounds are compared.

2. Hartree–Fock *ab initio* calculations

Experimental geometries of the TCNE molecule measured by electron diffraction in the gas phase (Hope, 1968) and by neutron diffraction in the cubic crystalline phase are reported in Table 1. At room temperature the cubic phase (Little *et al.*, 1971) of TCNE is body centered with the space group *Im*3 and three molecules per primitive cell. The cell parameter a is 9.736 (6) Å. The molecules are mutually perpendicular. This packing leads to the existence of a cavity centered at the site (0,0,0) (and its symmetry equivalent, $\frac{1}{2},\frac{1}{2},\frac{1}{2}$) and surrounded by a cage of six molecules, their double bonds pointing towards the center of the cavity (Fig. 1). The molecular in-plane bond angles C—C—C and C—C≡N are smaller in the solid state than in the isolated molecule and take the values 116.17 and 177.93°, respectively. The intramolecular non-bonding distance N···N is 0.11 Å lower than that in the molecule in the gas phase.

The crystal structure of the insertion compounds has not yet been solved. However, owing to the presence of a large hole in the cubic cell, we may postulate that the inserted atoms K or Na sit on the unoccupied sites. The nearest atoms are N atoms of the N≡C—C—C≡N groups. The distance N···N between two molecules on opposite faces is 7.14 Å, four times the van der Waals radius of N. Therefore, it is likely that alkali-metal inclusion will not modify the crystal space group *Im*3. Thus, assuming that the chemical formula is $X(\mathrm{TCNE})_3$, there is only one degree of freedom: the cell parameter. Alkali-metal atoms are electron donors and TCNE is an electron acceptor, so one can expect charge transfer between them. The symmetric arrangement around the cavity leads to a maximum transfer of one-third of an electron per molecule, and metallic properties might result from such a mechanism.

We carried out a Hartree–Fock geometry optimization for the isolated molecule using the *GAUSSIAN* package of programs (Biosym Technologies, 1993). Calculations were carried out with a standard Huzinaga–Dunning polarized double-zeta basis set. The results are shown in Table 1. The Hartree–Fock results reproduce the electron diffraction data quite well.

This molecular geometry being fixed, we optimized the cell parameter of cubic TCNE with the *CRYSTAL* package of programs (Dovesi *et al.*, 1994). The basis sets used were different from those of the molecular calculation: 6-31G* for C and N atoms. As noted by Dovesi, the use of standard basis sets with diffuse orbitals (like double zeta or triple zeta) has several drawbacks; these functions give rise to a high computational cost, large overlaps and pseudo-linear dependence between basis functions which leads to a catastrophic convergence behavior. Moreover, the true basis sets for a crystalline calculation are Bloch functions which are extended through the crystal; thus diffuse functions are unnecessary.

The cohesive energy *versus* the cell parameter for cubic TCNE is shown in Fig. 2. The optimized cell parameter is 9.98 Å, 2% above the experimental value,

and the cohesive energy is 38.5 kcal mol^{-1} (1 kcal mol^{-1} = 4.184 kJ mol^{-1}). This overestimate comes from the neglect of dispersive interactions. We also carried out a calculation with the experimental crystal-structure geometry, which leads to a value of 38 kcal mol^{-1} for the cohesive energy. Thus, we can conclude that the crystal environment has a negligible effect on the molecular geometry.

Hartree–Fock calculations for the insertion compounds (using *CRYSTAL*) were carried out with the optimized molecular geometry, 6-31G* basis sets for C and N atoms, 6-311G* for Na and 6-31G* modified by Ricart *et al.* (1995) for K.

The behavior of the cohesive energy *versus* cell parameter (Fig. 2) shows a minimum for the insertion compounds. Insertion of the alkali-metal atoms contracts the cell; this effect is less pronounced for K (9.96 Å) than Na (9.93 Å). The behavior of the interaction energies of the insertion compounds becomes unreasonable for large distances; this is characteristic of the Hartree–Fock inability to reproduce dissociation phenomena.

The Fock matrix was diagonalized at 39 points of the irreducible Brillouin zone for cubic TCNE and its insertion compounds. Cohesive energies were calculated with the counterpoise method of Boys & Bernardi (1970) to by-pass basis-set superposition errors (BSSEs).

3. Band structure and density of states

The valence configuration of the isolated molecule is $5A_g1B_{1u}1B_{2g}4B_{3g}1A_u4B_{1u}4B_{2u}2B_{3u}$. The HOMO ($B_{3u}$) is antibonding and is formed by the combination of the out-of-plane C≡N orbital and the π orbital of the ethylenic bond. The next occupied level (B_{3g} symmetry, 2.1 eV below the HOMO) is a bonding one and is built from the overlap between σ C≡N hybrids. The antibonding LUMO (B_{1g} symmetry), 10.3 eV above the HOMO, is mainly localized on the double bond and N. There is a charge depletion (revealed by a Mulliken population analysis) on the ethylenic C atoms owing to the high electronegativity of the cyanide groups. Consequently, the C=C group will play a major role in charge transfer mechanisms.

The band structure along special lines Δ, Λ, Σ, D, G and at special points H, P, N, Γ of the irreducible Brillouin zone (Fig. 3) and the density of states (DOS) of cubic TCNE are shown in Fig. 4. Cubic TCNE is an insulator with a large direct gap (about 10.2 eV) located at the point N of the Brillouin zone. The highest group of valence bands originate from the overlap between B_{3u} molecular orbitals and the second highest group from B_{3g} molecular orbitals. The lowest unoccupied band is built from the overlap between LUMOs and can be filled by six electrons. Band widths are narrow, as a

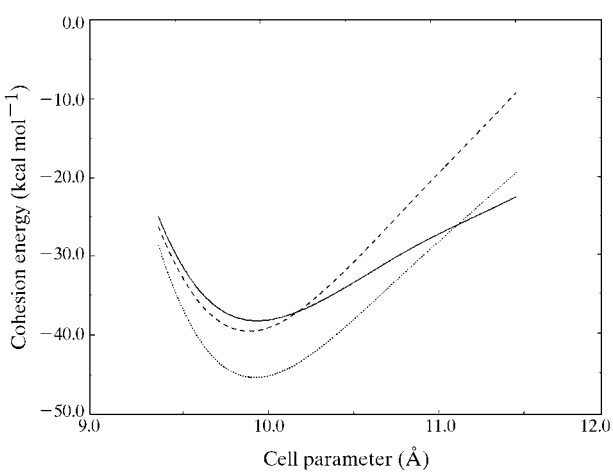

Fig. 2. Interaction energy *versus* cell parameter. Solid line: TCNE molecular solid; dotted line: K(TCNE)$_3$ crystal; dashed line: Na(TCNE)$_3$ crystal.

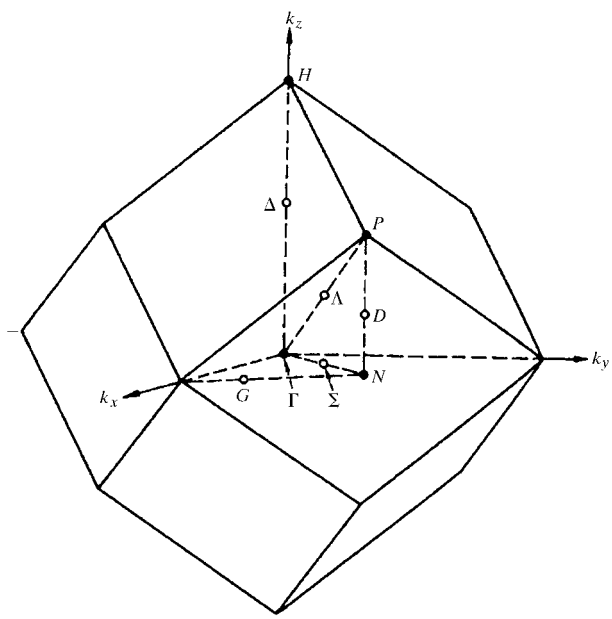

Fig. 3. The cubic cell Brillouin zone.

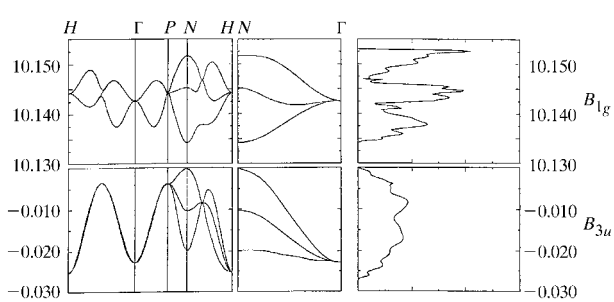

Fig. 4. Band structure of the TCNE molecular crystal. Energies are in eV and the Fermi level is at 0 eV.

result of both the low spatial extension of the molecular orbitals and the large size of the cell.

Mulliken partition of the DOS gives the atomic contributions in band formation. From the total DOS, $\rho_t(\varepsilon)$, one can define μ orbital DOS, $\rho_\mu(\varepsilon)$, and atom A DOS, $\rho_A(\varepsilon)$, by

$$\rho_t(\varepsilon) = \sum_A \rho_A(\varepsilon)$$

$$\rho_A(\varepsilon) = \sum_{\mu \in A} \rho_\mu(\varepsilon)$$

$$\rho_\mu(\varepsilon) = (2/V_{\mathrm{BZ}}) \sum_j \sum_\nu \sum_{\boldsymbol{g}} \int_{\mathrm{BZ}} \{d\boldsymbol{k} S_{\mu\nu}(\boldsymbol{k}) a_{\mu j}(\boldsymbol{k}) a^*_{\nu j}(\boldsymbol{k}) e^{i\boldsymbol{k}\cdot\boldsymbol{g}} \delta \times [\varepsilon - \varepsilon_j(\boldsymbol{k})]\},$$

where $\boldsymbol{k}$ is the wave vector, $\boldsymbol{g}$ is a direct space vector, V_{BZ} is the volume of the Brillouin zone, $S(\boldsymbol{k})$ is the overlap matrix, $a_{\alpha m}$ is the wave-function coefficient for band m and orbital α, j is an index of the band and greek letters represent atomic orbitals (Dovesi *et al.*, 1994).

By restricting j values to a limited set of bands, one can define a partial atomic DOS. With knowledge of this quantity, one can estimate the covalent and ionic characters of the interactions in the crystal. In the case of the insertion compounds, a covalent character of interaction between molecules and inserted atoms will appear as a non-zero contribution of the inserted atom to the partial atomic DOS limited to the conduction bands.

From Fig. 5, we can see that the B_{3u} and B_{1g} bands have major contributions from C_1 and N atoms (C atoms of ethylenic bonds are designated by C_2, C atoms of single bonds by C_1).

Inclusion of alkali-metal atoms affects the band structure (Figs. 6*a* and 6*b*) leading to metallic conduction; the DOS becomes non-zero at the Fermi level, associated with a charge transfer from the alkali-metal valence orbital to the first unoccupied bands of the molecular solid. The global atomic contributions to the DOS (Fig. 7 compared with Fig. 5) are not strongly modified by charge transfer, so the conduction bands in the insertion compounds remain B_{1g}, confirming the transfer to the C_2 atoms. The atomic DOS for the inserted atoms is only significant for B_{3g} bands.

In the vicinity of the Γ point, the conduction bands for the two insertion compounds are quite different, although the valence bands are rather similar. The difference is probably related to the different size of the 2*p* and 3*p* orbitals of the Na and K atoms, respectively.

The conduction mechanisms in the insertion compounds are highly connected with the symmetry equivalence of the three TCNE molecules in the unit cell. If the inclusion of alkali-metal atoms does not modify the crystal symmetry, there should be no symmetry breaking of local degeneracy for the three unoccupied bands at special points of the Brillouin zone. Consequently, there are three conduction bands in each insertion compound (constructed from combination of the LUMOs) strongly localized on double ethylenic bonds, as one can see by inspection of the atomic DOS.

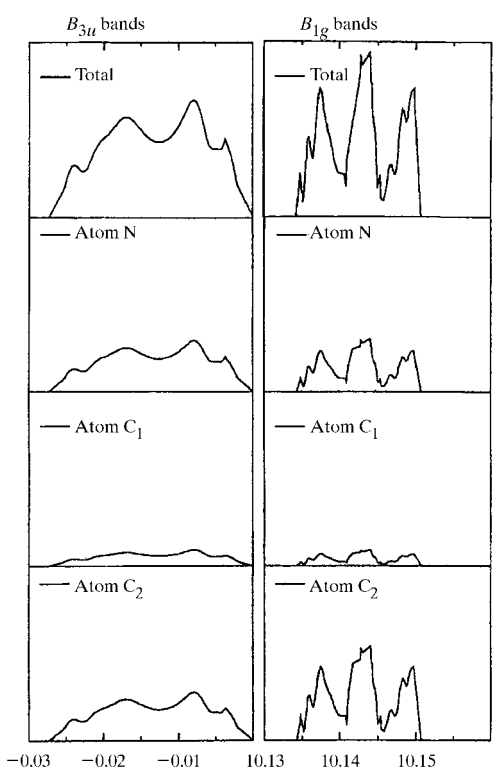

Fig. 5. Total and atomic density of states for the TCNE molecular crystal. Full scale for DOS, energies are in eV and the Fermi level is at 0 eV.

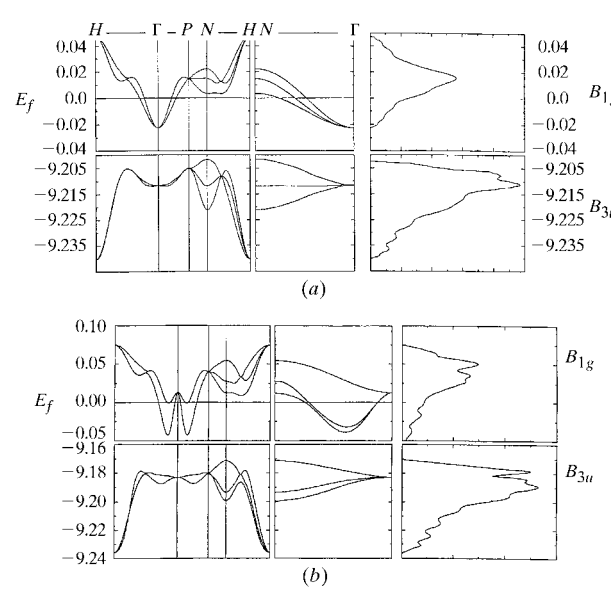

Fig. 6. (*a*) Band structure of the $K(TCNE)_3$ crystal. Energies are in eV and the Fermi level is at 0 eV. (*b*) Band structure of the $Na(TCNE)_3$ crystal. Details as part (*a*).

Crossings of these bands at special points reflect the possibility that the electron can hop from one molecule to another. We will return to this problem in the next section.

4. Electron densities in molecular crystals and inclusion compounds

Charge and momentum electron densities are well defined quantities which are observable and fundamentally related to the ground state by virtue of the Hohenberg–Kohn theorem. They respond in a complementary way to physical effects: charge density reveals localized effects of atomic interactions, momentum density is more sensitive to diffuse and collective effects. Thus, a combined analysis of these quantities should provide complementary views of electron behavior. One is interested in changes of densities induced by atomic interactions. The commonly used function in real space is the difference between the total density of a system and the pro-molecule density (the sum of the densities of non-interacting elements of the system), the so-called deformation density. Another significant quantity in momentum space is the Compton anisotropy, *i.e.* the difference between two directional profiles.

Other useful density differences can be defined in molecular crystals or charge transfer complexes:

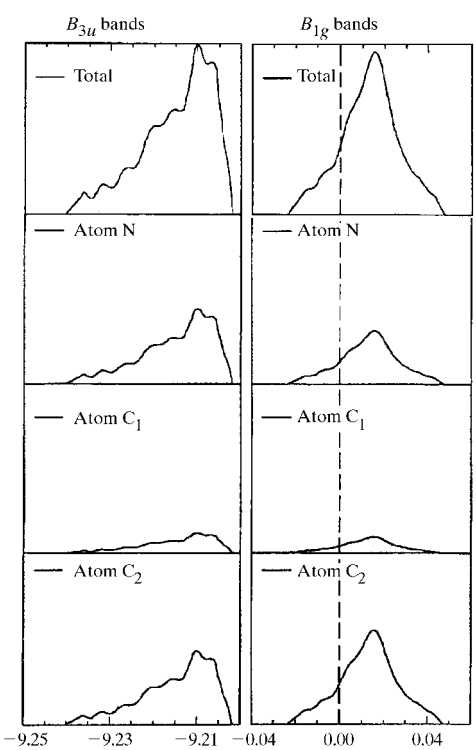

Fig. 7. Total and atomic density of states for the $K(TCNE)_3$ crystal. Full scale for DOS, energies are in eV and the Fermi level is at 0 eV.

(i) The interaction charge density. In molecular crystals, this is the difference between the total density of the crystal and the sum of the densities of the non-interacting molecules. This function describes electronic redistribution effects induced by crystal formation. For insertion compounds, physical effects of interest are the perturbations induced by the insertion process on the electron density around molecular regions in the unit cell. This information is revealed by the second-order interaction charge density calculated as the difference between the insertion compound total density and the molecular solid total density augmented by that of the inserted atom.

(ii) For the molecular solid, the interaction profile is calculated by subtracting isotropic molecular Compton profiles from the crystal phase profile (each being normalized to the total number of electrons). By subtracting the valence isotropic Compton profile of the included atom from this last quantity, one obtains in momentum space an equivalent of the interaction charge density. Owing to the sensitivity of Compton

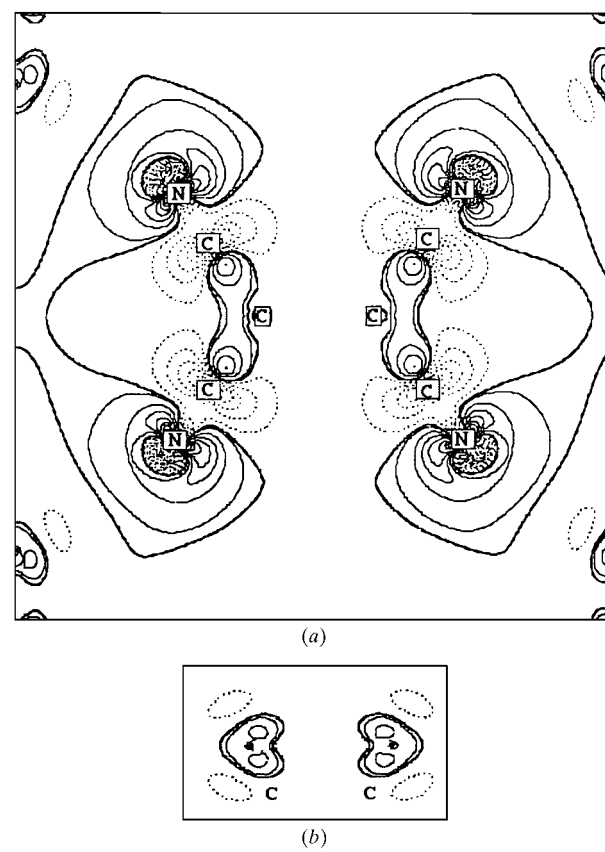

Fig. 8. (*a*) Interaction density of the TCNE cubic crystal in the molecular plane. Contours are at 0.005 e $Å^{-3}$; dotted lines are negative contours, solid thin lines are positive contours and solid thick lines are null contours. (*b*) Interaction density of the TCNE cubic crystal in the π plane through the ethylenic bond. Contours as part (*a*).

analysis to diffuse effects, interaction profiles of the insertion compounds should give useful information about the spatial extent of the atomic orbitals and conduction bands of the crystal.

Here we present theoretical estimations of these functions. All calculations have been carried out with the same basis set in order to by-pass BSSEs (Boys and Bernardi counterpoise method).

4.1. *Interaction charge densities of the molecular crystal and insertion compounds of TCNE*

(*a*) In the molecular cubic crystal, molecules possess a center of symmetry and interact *via* quadrupole–quadrupole and dispersive interactions. Owing to the large unit cell and weak overlap between molecular orbitals, the exchange interaction energy is negligible (Belemlilga, 1997).

The present Hartree–Fock charge density is mainly sensitive to the polarization contribution to intermolecular interactions. Interaction charge densities in molecular σ and π planes are shown in Figs. 8(*a*) and 8(*b*). In the σ plane (Fig. 8*a*), the interaction density is positive along the C—C single bond, and negative along the cyanide bond and near the N atoms in the lone-pair region. In the π ethylenic plane (Fig. 8*b*) positive contours are localized on the C atoms.

The structure of the interaction charge density is understood when we look at the molecular packing in the crystal (Fig. 9). The ethylenic bond of each molecule is surrounded by four N≡C—C=C—C≡N groups belonging to neighboring molecules. Consequently, charge depletion on the ethylenic bond of each molecule acts as a source of an attractive potential on the highly polarizable cyanide bonds of the nearest molecules. Thus, there is a density flow towards internal regions of the molecule and a decrease along the triple bond. These crystal-environment effects are weak; the highest peak of interaction density is 0.05 e Å^{-3} and is localized in the lone-pair region.

(*b*) The interaction densities of the insertion compound $K(TCNE)_3$ are shown in Figs. 10 and 11 for the σ and π molecular planes, respectively [the results for $Na(TCNE)_3$ are similar]. Around the inclusion site, there is a contraction of the alkali-metal core density due to charge transfer. Indeed, the ionization of the alkali-metal-atom valence orbital weakens the screening of electrons and increases the density near the nucleus.

In the σ plane (Fig. 10), charge density decreases along the double bond, in the vicinity of the N-atom positions and in the lone-pair regions. The interaction density is positive along the cyanide bond and external molecular zones, and is also polarized towards the cation. Density for the two charge transfer complexes is globally negative in the σ plane.

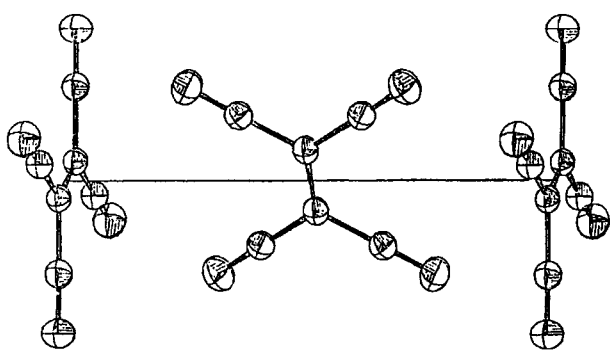

Fig. 9. Molecular packing in the cubic cell of TCNE.

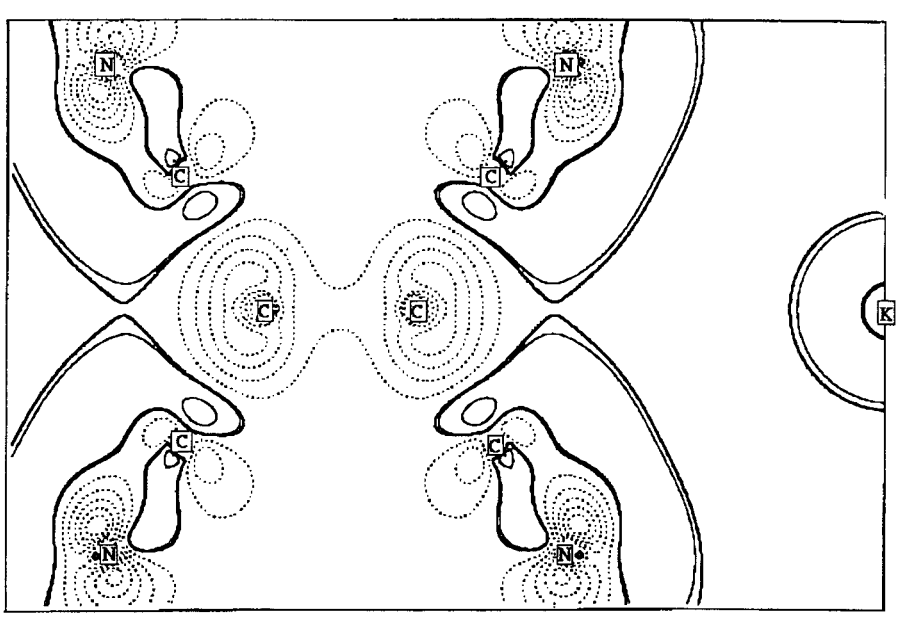

Fig. 10. Interaction density of the $K(TCNE)_3$ crystal in the molecular plane. Contours are at 0.01 e Å^{-3}. Dotted lines are negative contours, solid thin lines are positive contours and solid thick lines are null contours.

In the π plane (Fig. 11), the contours of the interaction density are positive on the C atoms and polarized towards the cations.

Interaction density contours are localized around the molecules and the included atoms. There are no characteristic contours of overlap between the alkali metals and the molecules. This is a confirmation of the strongly ionic character of the interactions between the molecules and the included atoms. Electrostatic attraction by the cations polarizes the density towards the inclusion site and charge transfer leads to a density flow between the σ and π planes. The nature of the included atom is only important in its immediate neighborhood. Around the molecules, the interaction density shows the same behavior for the two insertion compounds. There is no evidence of different amounts of charge transfer for $K(TCNE)_3$ and $Na(TCNE)_3$.

4.2. *Compton profiles of the molecular crystal and insertion compounds*

We have also calculated normalized-to-one-electron Compton profiles of the molecular crystal and inclusion compounds along the most important crystallographic directions [100], [110] and [111] of the conventional cell.

Compton anisotropies (the difference between two directional Compton profiles) are weak (with respect to the present experimental accuracy) both for the molecular cubic crystal and its insertion compounds. They are not plotted here. Molecules with three orthogonal orientations are present along each axis (Fig. 1), leading to the same induced averaged intermolecular interaction perturbations on the momentum density (Belemlilga, 1997).

The difference between the isotropic valence profiles of the cubic crystal and the gaseous phase (the interaction profile) is the equivalent in momentum space of interaction charge density for the molecular solid. The results obtained (Fig. 12) show the weakness of diffuse effects in the electronic redistribution: the greatest peak, at 0.8 a.u., is about 0.2% of the highest value of the isotropic profile at $q = 0$. One can conclude that polarization and density flow observed by inspection of interaction charge density are the essential features of the crystalline effect.

Interaction profiles of the insertion compounds $X(TCNE)_3$ are shown in Fig. 13(a). These quantities exhibit two peaks for low and medium momentum transfers for each complex. The qualitative behavior of the $K(TCNE)_3$ and $Na(TCNE)_3$ interaction profiles are identical. Compared with real space, the effects revealed by Compton analysis are pronounced (about three times the value at $q = 0$ of the normalized isotropic valence Compton profile of the molecular crystal) and should be measurable. These features can be understood better by inspection of the isotropic Compton profiles for the TCNE LUMO and the alkali-metal valence orbitals (Fig. 13b). The LUMO profile was calculated by formally assuming an occupation by one electron in the neutral molecule. One can see that the K and Na valence profiles are sharper with higher amplitudes for low momentum transfers. This means that alkali-metal valence orbitals are more diffuse than the molecular LUMO. The apparent contraction of the LUMO comes from its localization on the double ethylenic bond. Thus, interaction Compton profiles essentially show the modification of orbital symmetry of the transferred electron.

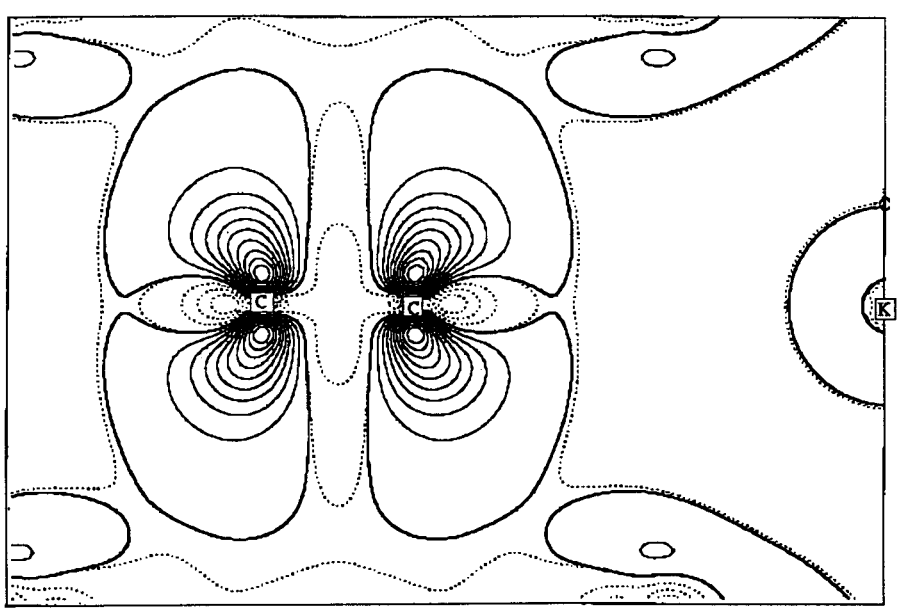

Fig. 11. Interaction density of the $K(TCNE)_3$ crystal in the π plane through the ethylenic bond. Contours as in Fig. 10.

The difference between the normalized isotropic valence profiles of cubic TCNE and the insertion compounds turns out to be weak (0.1% of the highest value of the normalized-to-one cubic TCNE isotropic profile). We can again conclude that the polarization and density flow (which are localized effects by nature) revealed by the interaction charge density are the essential features of charge transfer perturbations on the electron density of TCNE molecules.

As a conclusion of the band-structure study, we propose a Kronig–Penney conduction mechanism in the insertion compounds. The interaction profiles confirm this point of view: they describe an electron transferred towards a narrow zone strongly localized on the ethylenic bonds. Distortion in momentum space, the Compton anisotropies of the insertion compounds and interaction charge densities show the ionic character of the interaction between the inserted atoms and the molecule, and the absence of diffuse effects in the charge transfer perturbation; polarization and density flow can be seen as essentially due to electrostatic attraction of the cation and anionization of the TCNE molecules (this is demonstrated in the next section).

4.3. *Cluster modeling for the insertion compounds*

As a result of electron density studies, it seems reasonable to explain electronic mechanisms in TCNE insertion compounds by interactions between cations and negatively charged molecules. Let us simply model insertion compounds by ionic clusters $(X^+)_2\mathrm{TCNE}^-$. Negative charge on the molecule simulates charge transfer and positive charge on the cation ensures electrostatic attraction. These clusters were calculated at the Hartree–Fock level using the *GAUSSIAN* package (Biosym Technologies, 1993) and standard polarized double-zeta Huzinaga–Dunning basis sets for C and N.

The resulting interaction charge densities (the density of the total cluster minus the neutral molecule density and the neutral alkali-metal atom density) are shown in Figs. 14(*a*) and 14(*b*). The contours of density are similar to those obtained by a solid-state calculation and reveal the same features of polarization and density flow between the σ and π planes. Globally, in the σ and π planes, the highest peaks for the clusters are three times those obtained for the solid-state calculation. These discrepancies come from two facts:

(i) Intermolecular interactions in the crystal phase (which can be modeled as attraction between C atoms of each ethylenic bond and neighboring molecular cyanide bonds) compete with electrostatic attraction of the cations.

(ii) The maximum charge transfer rate is one electron per molecule for clusters and one-third of an electron for the crystal.

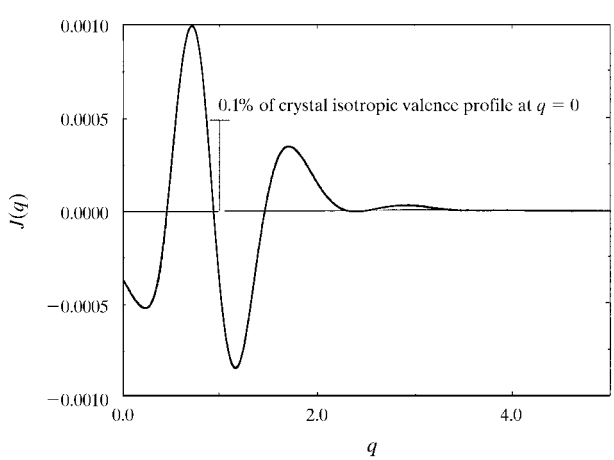

Fig. 12. Interaction profile of TCNE molecular solid. Each profile was normalized to one electron before calculating the difference.

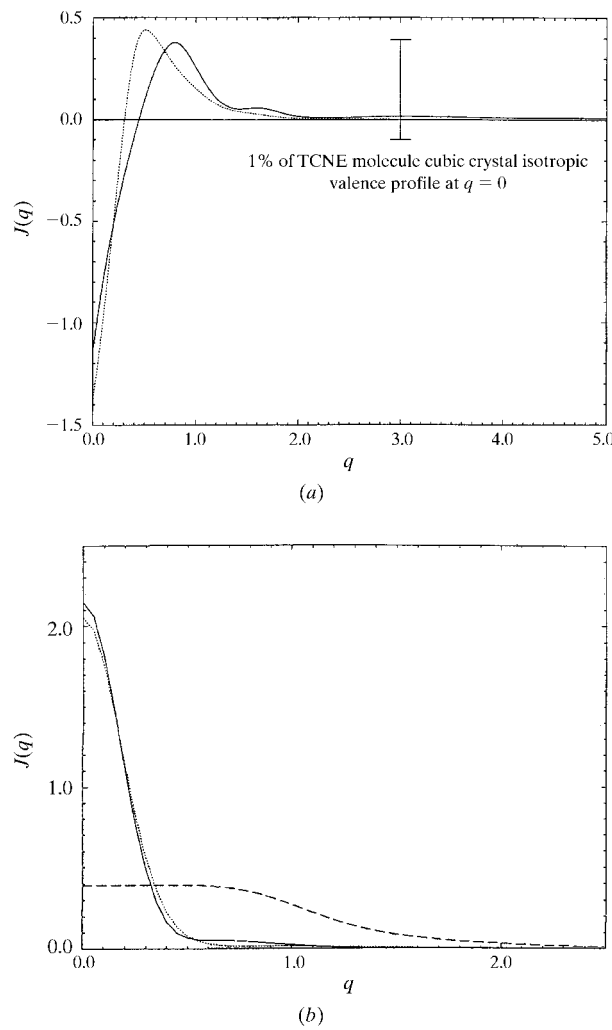

Fig. 13. (*a*) Interaction profiles in the insertion compounds. Solid line: $K(TCNE)_3$ crystal; dotted line: $Na(TCNE)_3$ crystal. (*b*) Compton profiles of alkali-metal-atom valence electrons and the TCNE LUMO. Solid line: 4*s* orbital of K; dotted line: 3*s* orbital of Na; dashed line: TCNE LUMO.

Similar conclusions can be drawn for momentum space analysis (see, for example, the interaction profile in Fig. 15).

As a conclusion, we claim that the behavior of the electron densities in real and momentum space for the insertion compounds is entirely governed by anionization of TCNE molecules and attraction by cations located on the inclusion site. Charge transfer strongly distorts the electron distribution and Coulomb attraction enhances these effects both in real and momentum space.

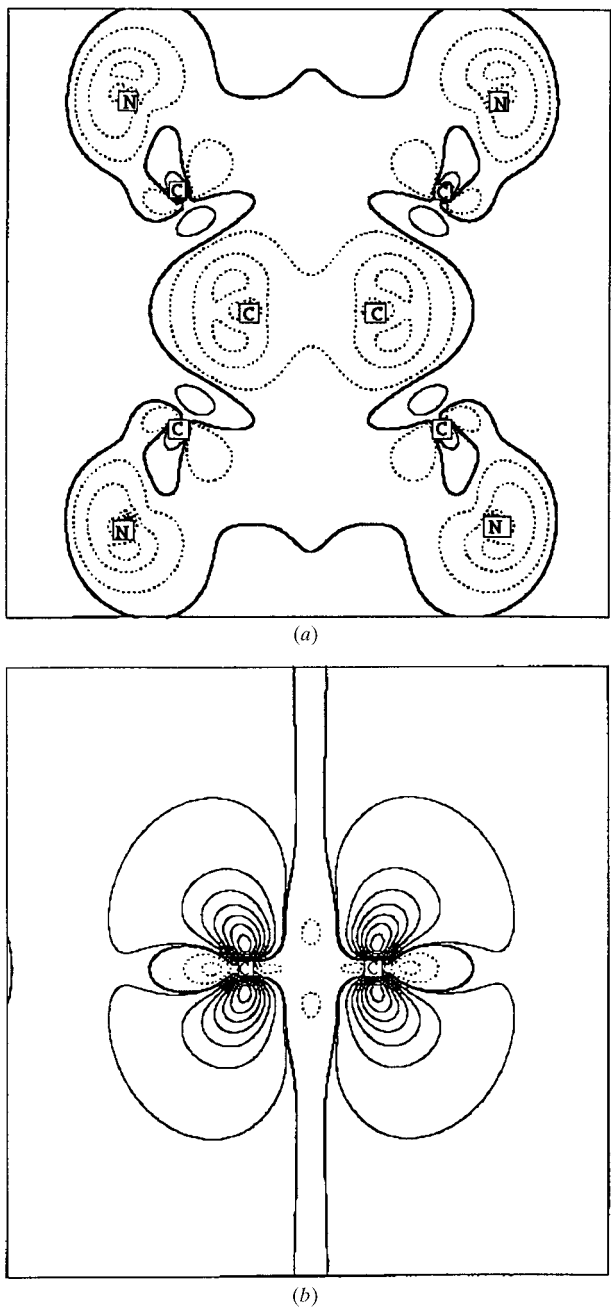

Fig. 14. (*a*) Interaction density in the molecular plane. Only the results for the cluster $(K^+)_2(TCNE)^-$ are shown. Contours are at 0.05 e Å^{-3}; dotted lines are negative contours, solid thin lines are positive contours and solid thick lines are null contours. (*b*) Interaction density in the π plane through the ethylenic bond. Details as part (*a*).

5. Conclusion and comparison with insertion compounds of C_{60}

In this paper we have shown that cubic TCNE can form energetically stable insertion compounds with alkali-metal atoms. A band-structure study of cubic TCNE and $X(TCNE)_3$ reveals a charge transfer between the alkali-metal atoms and the molecules in the crystal. Charge density analysis shows polarization and density flow effects in the solid state. These phenomena appear clearly in the interaction charge density. In momentum

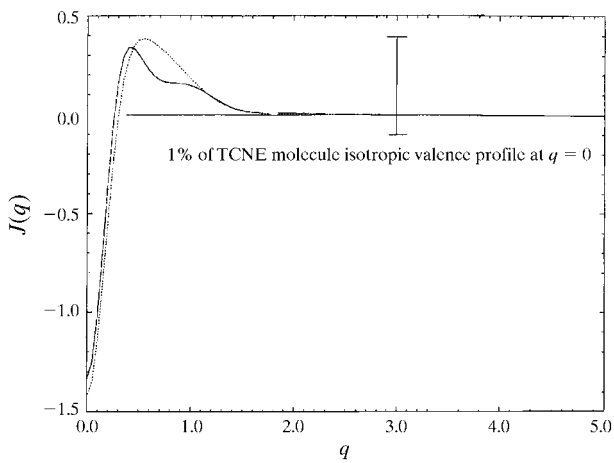

Fig. 15. Interaction profiles of the clusters $(X^+)_2(TCNE)^-$. Solid line: $(K^+)_2(TCNE)^-$ cluster; dotted line: $(Na^+)_2(TCNE)^-$ cluster.

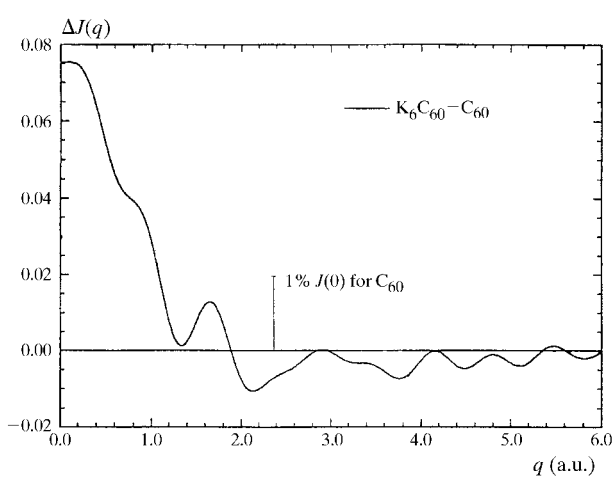

Fig. 16. The difference between the isotropic valence Compton profiles of K_6C_{60} and C_{60}.

space, similar functions calculated from Compton profiles allow for a detailed analysis of various characteristics of charge transfer such as the distortion of the valence electron distribution, the behavior of the transferred electron and symmetry properties. This combined analysis in real and momentum space validated our assumptions about the conduction mechanism in insertion compounds. The separate effects of charge transfer and electrostatic attraction on electron densities were studied with some simple models of TCNE insertion compounds.

Let us now conclude this paper with a brief comment on C_{60} and its insertion compounds. C_{60} is a face-centred cubic crystal of which 26% is empty volume. As in cubic TCNE, the C_{60} crystal possess unoccupied sites (two tetrahedral and one octahedral site per molecule). Solid C_{60} is an insulator with three unoccupied bands which can be filled with six electrons. There is another similarity between C_{60} and TCNE: the C_{60} molecule is characterized by a high electron affinity and has a tendency to form stable anionic states. Insertion of alkali-metal atoms in the crystal structure leads to a charge transfer towards the C_{60} molecules. With atomic K, C_{60} forms two complexes: an insulator K_6C_{60} and a superconductor K_3C_{60}. The former has a body-centred cubic structure, the latter remains face-centred cubic.

Moscovici *et al.* (1995) have measured the differences of isotropic valence Compton profiles of K_6C_{60} and C_{60} (Fig. 16). Compton profiles are normalized to 4.1 electrons for K_6C_{60} (corresponding to the number of valence electrons in the ionized C atom in each inclusion compound), and 4 electrons for C_{60}. In the same manner, we have calculated the difference between the isotropic valence profiles of $K(TCNE)_3$ (normalized to 4.43 electrons) and the TCNE molecular crystal (normalized to 4.4 electrons) (see Fig. 17). The greatest peak for $K(TCNE)_3$ represents 1% of the TCNE molecular crystal valence profile at $q = 0$ and is comparable to the results of Moscovici *et al.*, *i.e.* 1.5% of the C_{60} valence profile at $q = 0$.

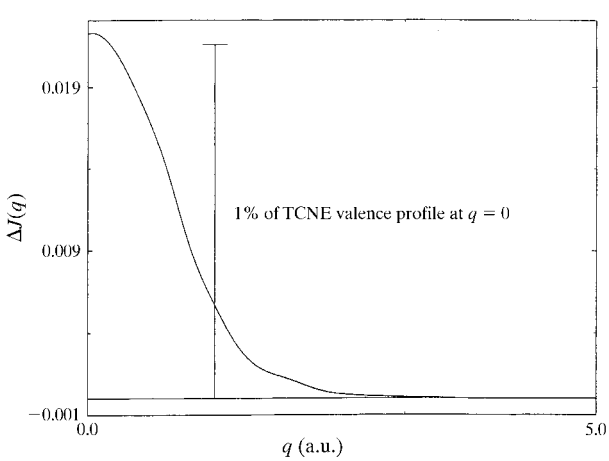

Fig. 17. The difference between the isotropic valence Compton profiles of $K(TCNE)_3$ and TCNE.

As noted in §1, metal salts of TCNE with K and Na (Webster *et al.*, 1962) exist and can be crystallized. We hope the present study has shown the interest in the synthesis and crystallization of these complexes and others which can be formed by the association of cubic TCNE and other molecules or atoms. This project will be continued in our laboratory.

The authors would like to thank Dr J. Moscovici and Professor Geneviève Loupias for making their results on fullerenes available, and Professor Pietro Cortona for useful discussions.

References

Becker, P. J., Coppens, P. & Ross, F. K. (1973). *J. Am. Chem. Soc.* **95**, 7604–7610.
Bekoe, D. A. & Trueblood, K. N. (1960). *Z. Kristallogr.* **113**, 1–22.
Belemlilga, D. (1997). Thesis, Université de Marne la Vallée, France.
Berg, T. H. M. van der & van der Avoird, A. (1989). *J. Phys. Condens. Matter*, **1**, 4047–4055.
Biosym Technologies (1993). *GAUSSIAN*. Version 2.3. Biosym Technologies, San Diego, USA.
Boys, F. S. & Bernardi, D. (1970). *Mol. Phys.* **19**, 553–566.
Chaplot, S. L., Mierzejewski, A. & Pawley, G. S. (1985). *Mol. Phys.* **56**, 115–128.
Chaplot, S. L., Mierzejewski, A., Pawley, G. S., Lefebvre, J. & Luty, T. (1983). *J. Phys. C.* **16**, 625–644.
Cioslowski, J. (1994). *Int. J. Quantum Chem.* **49**, 463–475.
Cioslowski, J., Mixon, S. T. & Edwards, W. D. (1991). *J. Am. Chem. Soc.* **113**, 1083–1085.
Czuchajowski, L., Pietrzycki, W. & Cicha-rozok, J. (1974). *Bull. Acad. Pol. Sci. Ser. Sci. Chim.* **22**, 225–233.
Dhar, D. N. (1967). *Chem. Rev.* **67**, 611–622.
Dovesi, R., Saunders, V. R. & Roetti, C. (1994). *CRYSTAL92 User Manual*. Theoretical Chemistry Group, University of Turin, Italy, and SERC Daresbury Laboratory, Warrington, England.
Edwards, W. D., Du, M., Royal, J. S. & McHale, J. L. (1990). *J. Phys. Chem.* **94**, 5748–5752.
Emery, L. C., Sheldon, J. M., Edwards, W. D. & McHale, J. L. (1992). *Spectrochim. Acta Part A*, **48**, 715–724.
Erwin, S. C. & Pederson, M. R. (1991). *Phys. Rev. Lett.* **67**, 1610–1613.
Erwin, S. C. & Pickett, W. E. (1991). *Science*, **254**, 842.
Hebard, A. F. (1991). *Nature*, **350**, 600.
Hope, H. (1968). *Acta Chem. Scand.* **22**, 1057–1058.
Levi, B. G. (1977). *Phys. Today*, **30**, 18–19.
Little, R. G., Pautler, D. & Coppens, P. (1971). *Acta Cryst.* B**27**, 1493–1499.
Looney, C. E. & Downing, J. R. (1958). *J. Am. Chem. Soc.* **80**, 2840–2844.
Matthews, D. A., Swanson, J., Mueller, M. & Stucky, G. D. (1971). *J. Am. Chem. Soc.* **93**, 5945–5953.

Mierzejewski, A. & Chaplot, S. L. (1980). *Proc. VIIth Intl. Conf. Raman Spectrosc.*, Edited by W. F. Murphy, p. 46. Amsterdam: North-Holland.
Moscovici, J. (1994). Thesis, Université Paris VI, France.
Moscovici, J., Loupias, G., Rabii, S., Erwin, S., Rassat, A. & Fabre, C. (1995). *Europhys. Lett.* **31**, 87–93.
Mukhopadhyay, R., Chaplot, S. L. & Rao, K. R. (1985). *Phys. Status Solidi A*, **92**, 467.
Murgich, J. & Pissanetzky, S. (1975). *J. Chem. Phys.* **62**, 92–93.
Ohno, T., Nakao, K. & Kanimura, H. (1979). *J. Phys. Soc. Jpn*, **47**, 1125.
Onda, S., Iluda, R., Nakamura, D. & Kubo, M. (1969). *Bull. Chem. Soc. Jpn*, **42**, 2740.
Regnault, A. (1986). Thesis, Université de Grenoble, France.
Ricart, J. M., Dovesi, R., Roetti, C. & Saunders, V. R. (1995). *Phys. Rev. B*, **52**, 2381–2389.
Tatar, R. C. (1985). PhD thesis, University of Pennsylvania, USA.
Vincenzo, D. P. & Rabii, S. (1982). *Phys. Rev. B*, **25**, 4110–4125.
Webster, O. W., Mahler, W. & Benson, R. E. (1962). *J. Am. Chem. Soc.* **84**, 3678–3684.